

SLAC – PUB – 3533  
December 1984  
(T/E)

SUPERSYMMETRIC EFFECTS IN  
POLARIZED-  $e^\pm - p$  SCATTERING\*

LUC MARLEAU<sup>†</sup>

*Stanford Linear Accelerator Center  
Stanford University, Stanford, California, 94305*

ABSTRACT

We study the polarization asymmetry in polarized- $e^\pm p \rightarrow e^\pm X$  scattering in supersymmetric quantum chromodynamics (SQCD). The main SQCD correction comes from the squark content of the proton which leads to  $\sim 10\%$  and  $\sim 15\%$  corrections for  $ep$  colliders at HERA ( $30 \text{ GeV} \times 820 \text{ GeV}$ ) and SSC ( $30 \text{ GeV} \times 20 \text{ TeV}$ ) respectively.

Submitted to *Physical Review D*

---

\* Work supported by the Department of Energy, contract DE – AC03 – 76SF00515.

† Address after June 1, 1985: Département de physique, Université Laval, Québec, P. Q., Canada, G1K 7P4.

## 1. Introduction

Despite its successes, few physicists believe that the standard  $SU(3) \times SU(2) \times U(1)$  gauge model is the ultimate theory of elementary particle interactions. Many reasons motivate that belief. There are too many parameters in the theory (at least 18, including coupling constants, fermion masses and mixings); the problem of fermion generations is not addressed; gravitation is absent, etc. Several attempts have been made to answer these questions. By far, the most intensively studied class of theories has been supersymmetry (SUSY).

Supersymmetry<sup>[1,2]</sup> is a natural extension of the standard gauge theories which exhibits the most attractive features of being less divergent and mathematically better behaved. In connection with grand unified theories (GUT) for example, these features play a vital role: SUSY permits the cancellation of quadratic divergences in the radiative correction to the mass of the Higgs boson and brings a satisfactory solution to the hierarchy problem that is plaguing standard GUT's. There is also hope that gravity could be included in a theory based on the invariance under local SUSY transformations.

SUSY predicts a whole new spectrum of particles, the superpartners, which differ by 1/2-spin with respect to their standard partners. Recently, the predictions of QCD regarding the  $Q^2$ -evolution of the structure functions have been extended to include effects of supersymmetric partons, i.e. gluinos and squarks,<sup>[3-5]</sup> in the framework of supersymmetric QCD (SQCD).

Apart from looking directly at the production of SUSY particles, it is instructive to examine the polarization effects in such a theory. After all, the supersymmetric extension changes the whole spin content of the theory and one

expects an indirect, if not direct, evidence of SUSY in polarized collisions. Perhaps the best place to look is in neutral current processes, especially in deep inelastic

$$e_{L,R}^- p \rightarrow e^- X . \quad (1.1)$$

In the past, this process has proven to provide a good test of the standard model and a way to determine the Weinberg angle.<sup>[6]</sup> The main SQCD contribution to this process is expected to come from the subprocess

$$e_{L,R}^- + \tilde{q} \rightarrow e^- + \tilde{q} \quad (1.2)$$

where  $\tilde{q}$  is a squark. Based on experiment and depending on the SUSY breaking mechanism, the mass of the squark is believed to be in the range  $20 \text{ GeV} \leq m_{\tilde{q}} \leq 100 \text{ GeV}$ . Only  $ep$  colliders such as HERA will be able to probe at  $Q^2$  sufficiently large to “see” the squark. Furthermore, the electron ring at HERA will have the ability to produce longitudinally polarized electrons when it starts running in 1990. The purpose of this paper is to study polarization effects attributable to the supersymmetric content in the proton in process (1.1). We also extend our calculations to the case of the positron-proton collisions.

The paper is organized as follows: Section 2 is devoted to preliminaries including the kinematics of  $ep$  scattering, the standard QCD predictions for electron-quark subprocesses and the definition of various polarization and charge asymmetries. In Section 3, we introduce the SQCD Lagrangian and compute the electron (positron) – squark contributions for HERA as well as an hypothetical  $ep$  machine at the Superconducting SuperCollider (SSC).<sup>[7]</sup> The numerical results are then discussed. Section 4 presents some general conclusions.

## 2. Preliminaries

The best available data on polarized- $eN$  scattering comes from the 1978 SLAC experiment which consisted of a 20 GeV electron beam on fixed targets.<sup>[6]</sup> Deuterons were then used as targets to eliminate uncertainties in the up- and down-quark distributions in the nucleon. Polarization asymmetries of the order of  $10^{-5}$  were detected in accordance with the standard model predictions.

At these energies, the dominant asymmetry comes from the interference of weak and e.m. currents and is of the order of  $O(Q^2/M_Z^2)$  where  $M_Z^2$  is the  $Z^0$  mass and  $Q^2$  is the square of the momentum transfer; the purely weak contributions are damped by an additional factor of  $Q^2/M_Z^2$ . Clearly, very high center-of-mass  $ep$  colliders would provide a better test of the standard model. The HERA proposal calls for 30 GeV electrons colliding with 820 GeV protons. Polarization in such an electron ring comes for free since it is expected to arise naturally due to a mechanism associated with quantum fluctuations in magnetic fields.<sup>[8]</sup> However, electron circular rings above 40 GeV are predicted to have little useful polarization. It is also interesting to study polarization asymmetries at an SSC facility (20 GeV protons) with 30 GeV polarized electrons.

If the incoming and scattered electrons have momenta  $p_1^\mu$  and  $p_3^\mu$  respectively, the proton has momentum  $p^\mu$  and partons has momentum fraction  $x$ , the usual kinematic variables are (see Fig. 1):

$$\begin{aligned}
s &= (p + p_1)^2, \\
Q^2 &\equiv -\hat{t} = -(p_3 - p_1)^2, \\
\nu &= p \cdot q / M_p, \\
x &= Q^2 / 2M_p\nu, \\
y &= Q^2 / xs,
\end{aligned} \tag{2.1}$$

where  $M_p$  is the mass of the proton.

The kinematics of deep inelastic scattering in  $ep$  collisions at both facilities is characterized by a strong domination by the proton motion. In general, this means that final states will be difficult to identify since such detection requires that the produced particles are sufficiently well separated from the beam. These experimental constraints impose stronger cuts on larger values of  $Q^2$ , which correspond to larger values of  $x$ .

Perhaps the most important limitation of the  $ep$  machines comes from their luminosity. Based on a somewhat optimistic assumption for the luminosity (i.e.  $\sim 10^{-32} \text{ cm}^{-2} \text{ sec}^{-1}$ )<sup>[9]</sup> one finds that it might be possible to study processes at the level of a fraction of a picobarn.

Consider now polarized- $ep$  scattering ( $e_{L,R}^- p \rightarrow e^- X$ ). At the parton level, the process is

$$e_{L,R}^- + q_i(\bar{q}_i) \rightarrow e^- + q_i(\bar{q}_i). \tag{2.2}$$

The fermion - vector-boson coupling can then be written as

$$\gamma_\mu = Q_{Rf}^V \gamma_\mu \left( \frac{1 + \gamma_5}{2} \right) + Q_{Lf}^V \gamma_\mu \left( \frac{1 - \gamma_5}{2} \right), \tag{2.3}$$

where  $Q_{Lf}^V$  and  $Q_{Rf}^V$  are the left- and right-handed charges of the fermion  $f$  associated with the vector-boson  $V$ . In the case of e.m. current alone, where

$$Q_{Lf}^\gamma = Q_{Rf}^\gamma = Q_f, \quad (2.4)$$

no polarization effect occurs except for those due to mass effects, which are very small. The standard model prescribes the following charges for the  $Z^0$ -fermion interactions:

$$Q_{Lf(Rf)}^Z = \frac{1}{\sin \theta_W \cos \theta_W} (I_{Lf(Rf)}^3 - Q_f \sin^2 \theta_W) \quad (2.5)$$

where  $I_{Lf(Rf)}^3$  is the third component of the weak isospin of the left- (right-) handed fermion and  $\theta_W$  is the Weinberg angle.

When a left- (right-) handed electron scatters from a left- (right-) handed parton, the cross section behaves as

$$\frac{d\hat{\sigma}_{AA}}{d\hat{t}} = \pi\alpha^2 \left| \frac{a}{\hat{t}} + \frac{b_{AA}}{\hat{t} - M_Z^2} \right|^2, \quad (2.6)$$

where

$$a = Q_e Q_i \quad (2.7)$$

$$b_{AB} = Q_{Ae}^Z Q_{Bi}^Z \quad A, B = L, R.$$

The left- (right-) handed electron on right- (left-) handed parton has a different  $y$ -dependence:

$$\frac{d\hat{\sigma}_{AB}}{d\hat{t}} = \pi\alpha^2 \left| \frac{a}{\hat{t}} + \frac{b_{AB}}{\hat{t} - M_Z^2} \right|^2 (1-y)^2, \quad A \neq B \quad (2.8)$$

with  $\hat{t} = -y\hat{s} = -xys$ .

For longitudinally polarized electron, it is then convenient to define the differential cross section

$$d\sigma_A^{(-)} \equiv \frac{d\sigma_A^{(-)}}{dxdy} = s \sum_i x f_i(x, Q^2) \frac{d\hat{\sigma}_{iA}}{d\hat{t}}. \quad (2.9)$$

Here  $f_i$  is the parton distribution in the proton,  $i$  runs over quarks and anti-quarks and  $d\hat{\sigma}_{iA}/d\hat{t}$  is the differential cross section for (2.2). Since the proton is unpolarized  $d\hat{\sigma}_{iA}/d\hat{t}$  involves an average over the left- and right-handed quarks.

It is easy to generalize (2.9) to positron-proton scattering; we denote the differential cross section by  $d\sigma_A^{(+)}$ . Following Ref. 10, we then define the polarization asymmetries  $A^\pm$  and  $B^{L,R}$

$$A^\pm(x, y) = \frac{d\sigma_R^{(\pm)} - d\sigma_L^{(\pm)}}{d\sigma_R^{(\pm)} + d\sigma_L^{(\pm)}} \quad (2.10)$$

$$B^A(x, y) = \frac{d\sigma_A^{(-)} - d\sigma_A^{(+)}}{d\sigma_A^{(-)} + d\sigma_A^{(+)}}. \quad (2.11)$$

The charge asymmetry for unpolarized  $e^\pm p \rightarrow e^\pm X$  scattering

$$C(x, y) = \frac{d\sigma^{(-)} - d\sigma^{(+)}}{d\sigma^{(-)} + d\sigma^{(+)}} \quad (2.12)$$

is also a useful tool to test the theory.

### 3. Supersymmetric QCD

We use the  $N = 1$  supersymmetric extension of the QCD Lagrangian<sup>[3-5]</sup>  
[11]

$$\begin{aligned}
\mathcal{L}_{\text{SQCD}} = & -\frac{1}{4}G_{\mu\nu}^a G^{a\mu\nu} + i\bar{q}_i \not{D} q_i + \frac{i}{2}\bar{\lambda}^a \not{D} \lambda^a + (D_\mu \tilde{q}_{iL})^\dagger (D^\mu \tilde{q}_{iL}) \\
& + (D_\mu \tilde{q}_{iR})^\dagger (D^\mu \tilde{q}_{iR}) - \frac{1}{2}g^2 \left( \tilde{q}_{iL}^\dagger T^a \tilde{q}_{iL} - \tilde{q}_{iR}^\dagger T^a \tilde{q}_{iR} \right)^2 \\
& + ig\sqrt{2} \left[ \bar{\lambda}_a \left( \frac{1+\gamma_5}{2} \right) \tilde{q}_{iL}^\dagger T_a q_i + \bar{\lambda}_a \left( \frac{1-\gamma_5}{2} \right) \tilde{q}_{iR}^\dagger T_a q_i - h.c. \right] \\
& + \text{mass terms} + \text{gauge fixing} + \text{Fadeev} - \text{Popov terms}
\end{aligned} \tag{3.1}$$

where  $G_{\mu\nu}^a$  is the gluon field strength,  $D_\mu$  is the covariant derivative and,  $q_i$  and  $\lambda^a$  stands for quarks and gluinos, whereas  $\tilde{q}_{iL(R)}$  are the squarks corresponding to their left- (right-) handed standard partners.  $T^a$  are the generators of SU(3) in the appropriate representation (gluons and gluinos are in the adjoint representation whereas quarks and squarks are in the fundamental representation). The indices  $i$  and  $a$  run over flavor and color respectively. Finally,  $g$  is the strong charge.

Recently, the Altarelli–Parisi equations have been extended to take into account the effects of supersymmetric partons<sup>[3-5]</sup> above their production thresholds. An interesting feature is that squarks are valence partons. Therefore, although their distribution increases slowly with  $Q^2$  and remain relatively small with respect to the quark distributions ( $\sim 5 - 7\%$ ), it becomes more important than the sea distributions for  $Q^2$  large enough. This is even more evident near  $x = 1$  since, in general, sea distributions are much steeper than valence distributions as  $x \rightarrow 1$ . Conversely, the ratio of  $f_{\tilde{q}}(x, Q^2)$  with respect to  $f_q(x, Q^2)$  is



quite insensitive to the value of  $x$ .

Consider the contribution of the subprocess

$$e_{L(R)}^{\pm} + \tilde{q}_i \rightarrow e^{\pm} + \tilde{q}_i . \quad (3.2)$$

We assume that all squarks are degenerate in mass and choose  $m_{\tilde{q}} = 20$  GeV. Using the Feynman rules for the  $\tilde{q}\tilde{q}\gamma$  and  $\tilde{q}\tilde{q}Z^0$  vertices as shown in Fig. 2,<sup>[12]</sup> it is easy to see that the cross section involving  $\tilde{q}_L$  and  $\tilde{q}_R$  have the same  $y$ -dependence.

One finds

$$\frac{d\hat{\sigma}_A}{d\hat{t}} = \pi\alpha^2 \left[ \left| \frac{a}{\hat{t}} + \frac{b_{AL}}{\hat{t} - M_Z^2} \right|^2 + \left| \frac{a}{\hat{t}} + \frac{b_{AR}}{\hat{t} - M_Z^2} \right|^2 \right] [(1-z)^2 - y] \quad (3.3)$$

for  $A = L$  or  $R$ . The variable  $z$  denotes the ratio  $M_q^2/\hat{s}$ . We construct the  $e^{\pm}p$  cross sections from the  $e^{\pm}$ -quark and  $e^{\pm}$ -squark cross sections (Eq. (2.6)–(2.8) and Eq. (3.3)) by folding with the parton distributions  $f_i(x, Q^2)$ .

The SQCD polarization asymmetries are calculated using the distributions of Kounnas and Ross<sup>[3]</sup> (KR). Here we choose somewhat arbitrarily:

$$Q^2 = -\langle \hat{t} \rangle_{\text{average}} = \frac{xs}{2}.$$

Unfortunately, KR do not compute the purely QCD distributions with the same set of assumptions. We must rely on other QCD distributions for comparison; we choose the parametrization of Glück, Hoffman and Reya<sup>[13]</sup> (GHR).

Figure 3 shows the results for the polarization asymmetry in  $e_{L,R}^- P \rightarrow e^- X$  for  $x = 1/3$  at energies  $\sqrt{s} = 314$  GeV (30 GeV  $\times$  800 GeV at HERA) and  $\sqrt{s} = 1550$  GeV (30 GeV  $\times$  20 TeV at SSC). The standard model prediction is

represented by the dotted (dashed) curve for HERA (SSC) whereas the solid (dot-dashed) curve shows the calculations taking into account the squark content of the proton as described by the KR distributions. There is essentially a discrepancy of  $\sim 9\%$  ( $\sim 10\%$ ) for most of the  $y$  range between both predictions. The case of  $e_{R,L}^+ p \rightarrow e^+ X$  scattering is illustrated on Fig. 4. Here, the supersymmetric effects are more important at small  $y$ 's, i.e. 9% for HERA and up to 7% for an SSC  $ep$  collider. Fortunately, this turns out to be the region of  $y$  where the experimental accuracy is best. For HERA, the discrepancy between SQCD and QCD gets large near  $y = 1$  but this region is completely inaccessible experimentally, the cross sections being too small.

As mentioned above, the detectors limitations at small angles with respect to the beam line imposes cuts on both regions of large and very small  $Q^2$ 's. However, in this case, we need not to be concerned with these bounds. Clearly, if the effects of the squark content in hadrons are to be seen, one must probe with  $Q^2 \gg 4M_q^2$  which is a much stronger constraint than the experimental one. Furthermore, most of the events will not escape the detector in the forward direction with respect to the proton beam, since the cross section is peaked at small  $Q^2$ . Therefore, although the cross sections are small, the rates should be sufficient to permit a analysis of the shape of the polarization asymmetry in a restricted region of  $x$  and  $y$ . The higher bounds on  $x$  and  $y$  can be estimated as follows: Assuming an accuracy of a few picobarns in the determination of the cross section, a discrepancy of 10% in the asymmetry would require that  $Q^2 \lesssim s/6$  in order to be detected at HERA ( $\lesssim s/18$  at SSC). For example, in our case ( $x = 1/3$ ), a 10% deviation from the standard model prediction in the polarization asymmetries,  $A^-$  and  $A^+$ , would be detectable for values of  $y$  as

large as .5 at HERA and .15 at SSC.

Figure 5 shows the results for  $B^{R,L}$  as functions of  $y$  for  $x = 1/3$ . Supersymmetric effects have a better chance of being observed in  $B^L$  rather than in  $B^R$ , although  $B^R$  is substantially larger as  $y$  approaches unity. Finally, the charge asymmetry  $C$ , such as defined in (2.12), appears on Fig. 6. The supersymmetric effects on the asymmetry for unpolarized protons are shown to be rather important. At HERA, they are shown to be of the order of 16% and they become more important at an SSC energy, i.e. 25% .

In general, one can make three observations: First, for most of the  $y$ -range (and certainly for the region of  $y$ 's where supersymmetric effects may be detectable) the squark content of the proton increases the absolute value of the polarization asymmetries. Furthermore, these effects seems to increase as the energy increases which is indicative of the  $Q^2$ -evolution of the squark distribution function in the proton. Second, the choice of  $x$  does not have a sizable effect on the asymmetries since the ratio of valence squark to valence quark distributions is not very sensitive to  $x$ . This is not the case, however, for the cross sections which, as one can see from equations (2.6), (2.8) and (3.3), are steep functions of  $x$  as well as of  $y$ . In that regard, the choice of  $x$  is moderate since in terms of parton distributions alone, the region of  $x$  that dominates is expected to be at  $x$ 's smaller than  $1/3$ . Finally, for  $x$  and  $y$  not too small the mass of the squark could be neglected in (3.3). For example, for  $x = .1$ ,  $z = .04$  and  $.0017$  at HERA and SSC energies respectively. Of course, for squark masses much larger than 20 GeV, say 100 GeV, the squark parton content decreases significantly, especially at HERA energies where polarization asymmetries would have no hope of being detected.

## 4. Conclusion

With HERA being built with a polarized electron beam, the process  $e_{R,L}^{\pm}p \rightarrow e^{\pm}X$  will certainly be the most thoroughly investigated and should give us a much better idea of the extent to which the standard model can be trusted. Modifications to the weak interaction theory (e.g. a second  $Z_0$ , composite structure at higher scale, superweak extension...) are also bound to show up in the asymmetries.

Our calculations leads to a squark content effect in polarization asymmetries of the order of 10% , detectable at both HERA and SSC. The evidence of supersymmetric QCD is even stronger if supported by a corresponding deviation in the charge asymmetry  $C$ . Of course, we have assumed a most optimistic scenario where the squark mass is only 20 GeV whereas, for most SUSY breaking mechanism, it may range from 20 to 100 GeV. Clearly, for  $M_{\tilde{q}}$  significantly larger than 20 GeV the effects would be difficult to detect. There is also little hope of addressing the question of the shape of the squark distribution in the proton but, this experiment should give an idea of the order of magnitude of the distribution, or bounds on the mass of the squark.

The  $ep$  machines such as HERA, are certainly not the first or even the best available experiment to test the existence of SQCD partons. In terms of the center-of-mass energy required to produce SUSY particles, both  $e^+e^-$  and  $\bar{p}p$  machines should reach HERA's capabilities before it comes in operation and, it is believed by most high energy physicists that the best signal for SUSY could come from missing  $p_T$  analysis. But missing  $p_T$ 's are certainly not exclusive to supersymmetric processes and one must look for other manifestations of SUSY. Furthermore, polarized-  $e^{\pm}p$  scattering is perhaps, the best way to test the weak

properties of such new partons. It is for these reason that we believe that this work is important.

### **ACKNOWLEDGEMENTS**

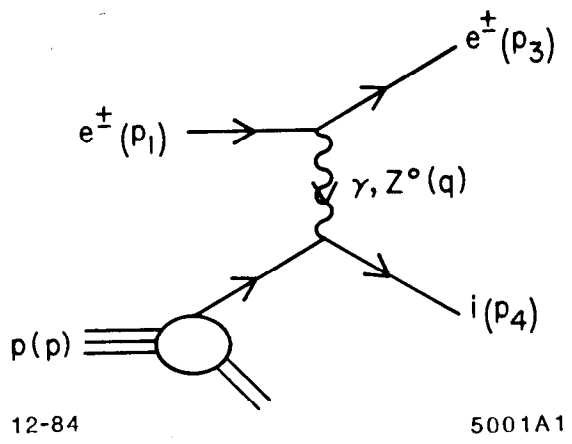
The author would like to thank Professor S. D. Drell and the other members of the Theory Group for their hospitality at SLAC. Many thanks also goes to E. Massó for useful suggestions in preparing the manuscript. This work was supported by the U.S. Department of Energy and the National Sciences and Engineering Research Council of Canada.

## REFERENCES

1. J. Wess and B. Zumino, Nucl. Phys. B70, 39 (1974); P. Fayet and S. Ferrara, Phys. Rep. 32C, 249 (1977).
2. P. Fayet and J. Iliopoulos, Phys. Lett. 51B, 461 (1974); E. Witten, Nucl. Phys. B188, 513 (1981); S. Dimopoulos and H. Georgi, Nucl. Phys. B93, 150 (1981).
3. C. Kounnas and D. A. Ross, Nucl. Phys. B214, 317 (1983).
4. S. K. Jones and C. H. Llewellyn Smith, Nucl. Phys. B217, 145 (1983).
5. I. Antoniadis, C. Kounnas and R. Lacaze, Nucl. Phys. B211, 216 (1983).
6. C. Y. Prescott et al., Phys. Lett. 77B, 347 (1978); 84B, 524 (1979).
7. S. Wojcicki, et al., Report of the 1983 Subpanel on New Facilities for the U.S. High Energy Program of the High Energy Physics Advisory Panel. (U.S. Department of Energy, Washington, 1983).
8. A. Sokelov and I. Ternov, Sov. Phys. Dokl., 8,1203 (1964).
9. J. Bagger and M. Peskin, Exotic Processes in High Energy  $e - p$  Collisions, SLAC preprint (SLAC-PUB-3447 T/E), Sept. 84, (to be published in Phys. Rev.); C. Y. Prescott, The  $ep$  Option at SSC, SLAC preprint (SLAC-PUB-3345 N), May 84.
10. R. Rückl, Nucl. Phys. B234, 91 (1984).
11. I. Antoniadis, L. Beaulieu and F. Delduc, Z. Phys. C23, 119 (1984)
12. H. E. Haber and G. L. Kane, The Search for Supersymmetry: Probing Physics Beyond the Standard Model, University of Michigan Preprint (UMHE-TH-81-17) Jan. 84, (to be published in Phys. Rep.).
13. M. Glück, E. Hoffman and E. Reya, Z. Phys. C13, 119 (1982).

## FIGURE CAPTIONS

1. Kinematics of  $e^\pm p \rightarrow e^\pm X$  scattering:  $i$  is a charged parton.
2. Feynman rules for  $qq\gamma$ ,  $qqZ^0$ ,  $\tilde{q}\tilde{q}\gamma$  and  $\tilde{q}\tilde{q}Z^0$  vertices.  $Q_{Ai}^V$  are defined in (2.3).
3. Polarization asymmetry  $A^-(x, y)$  in  $e_{L,R}^- p \rightarrow e^- X$  as a function of  $y$  for  $x = 1/3$ . The dotted and solid curves denote the prediction from QCD and SQCD respectively for the  $ep$  machine at HERA ( $\sqrt{s} = 314$  GeV); the dashed and dot-dashed curves are for the corresponding predictions for an SSC machine ( $\sqrt{s} = 1550$  GeV)
4. Polarization asymmetry  $A^+(x, y)$  in  $e_{L,R}^+ p \rightarrow e^+ X$  as a function of  $y$  for  $x = 1/3$ . The notation is the same as in Fig. 3.
5. Asymmetries  $B^{R,L}(x, y)$  for  $x = 1/3$ . The lower set of curves represents results for  $B^L(x, y)$  whereas the higher set is for  $B^R(x, y)$ ; apart from that, the notation is the same as in Fig. 3.
6. Charge asymmetry  $C(x, y)$  in  $e^\pm p \rightarrow e^\pm X$  (see Fig. 3 for notation).

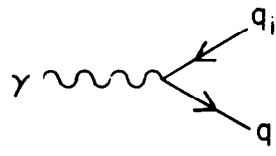


12-84

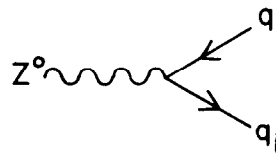
5001A1

Fig. 1

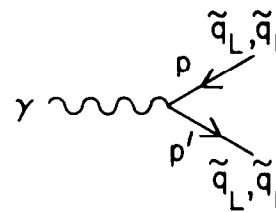




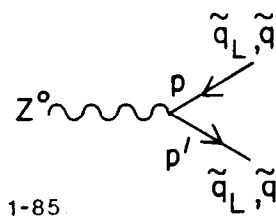
$$-ie Q_i^{\gamma} \gamma^{\mu}$$



$$-ie \left[ Q_{Ri}^Z \gamma_{\mu} \left( \frac{1+\gamma_5}{2} \right) + Q_{Li}^Z \gamma_{\mu} \left( \frac{1-\gamma_5}{2} \right) \right]$$

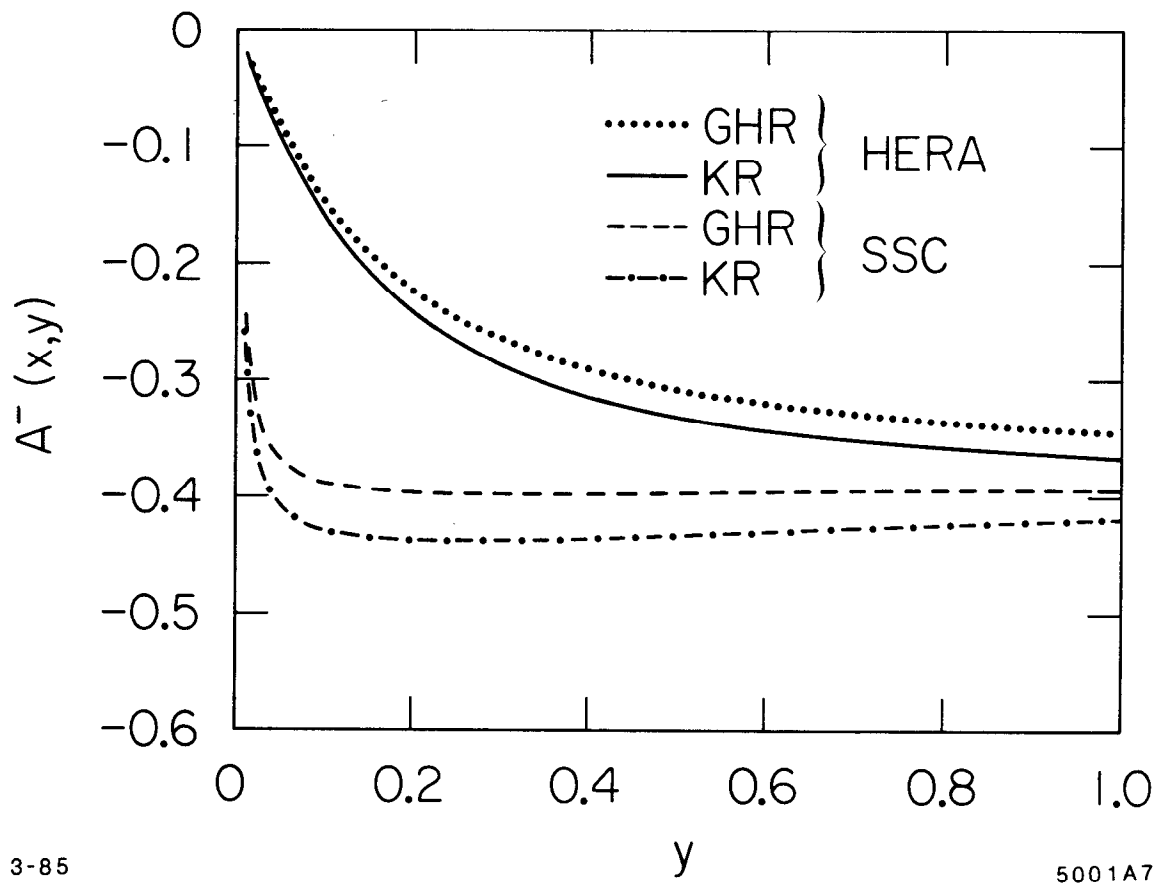


$$-ie Q_i^{\gamma} (p_{\mu} + p'_{\mu})$$



$$-ie Q_{Li,Ri}^Z (p_{\mu} + p'_{\mu})$$

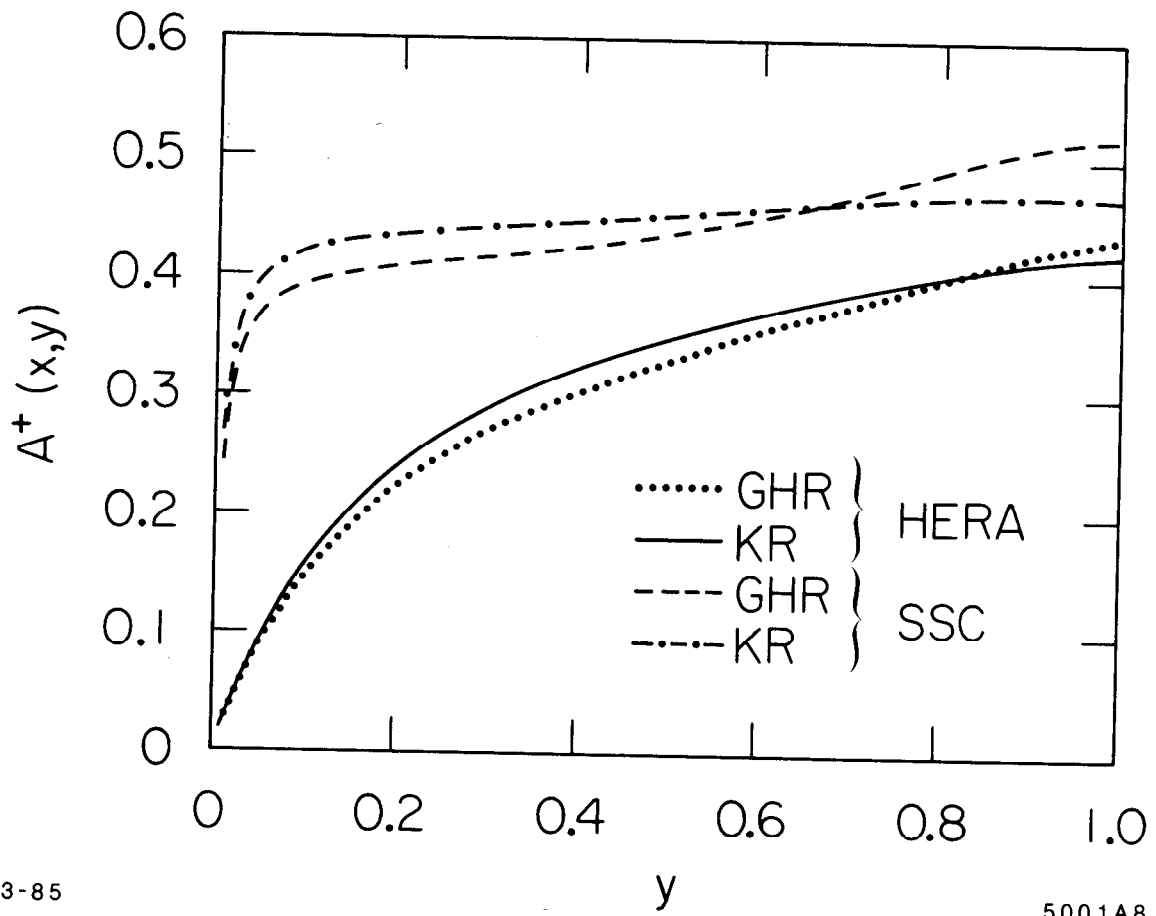
Fig. 2



3-85

5001A7

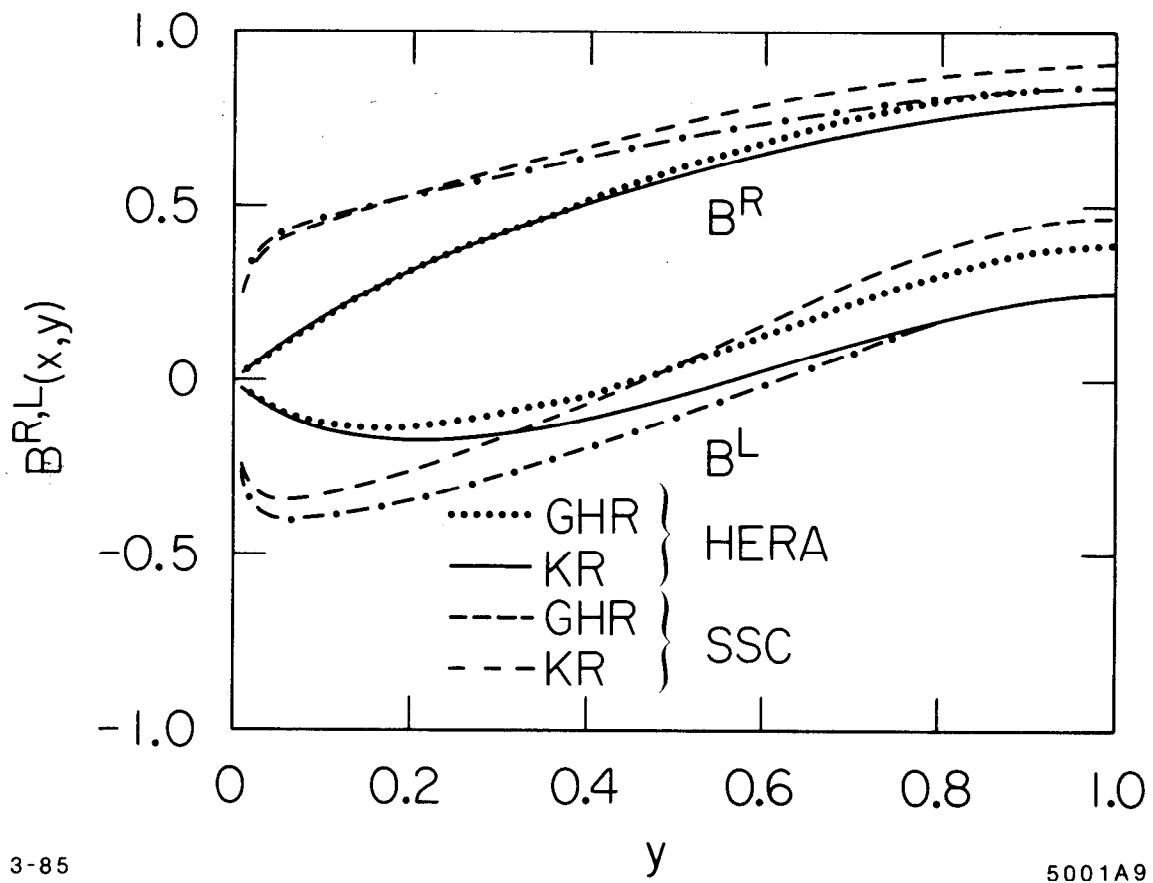
Fig. 3



3-85

5001A8

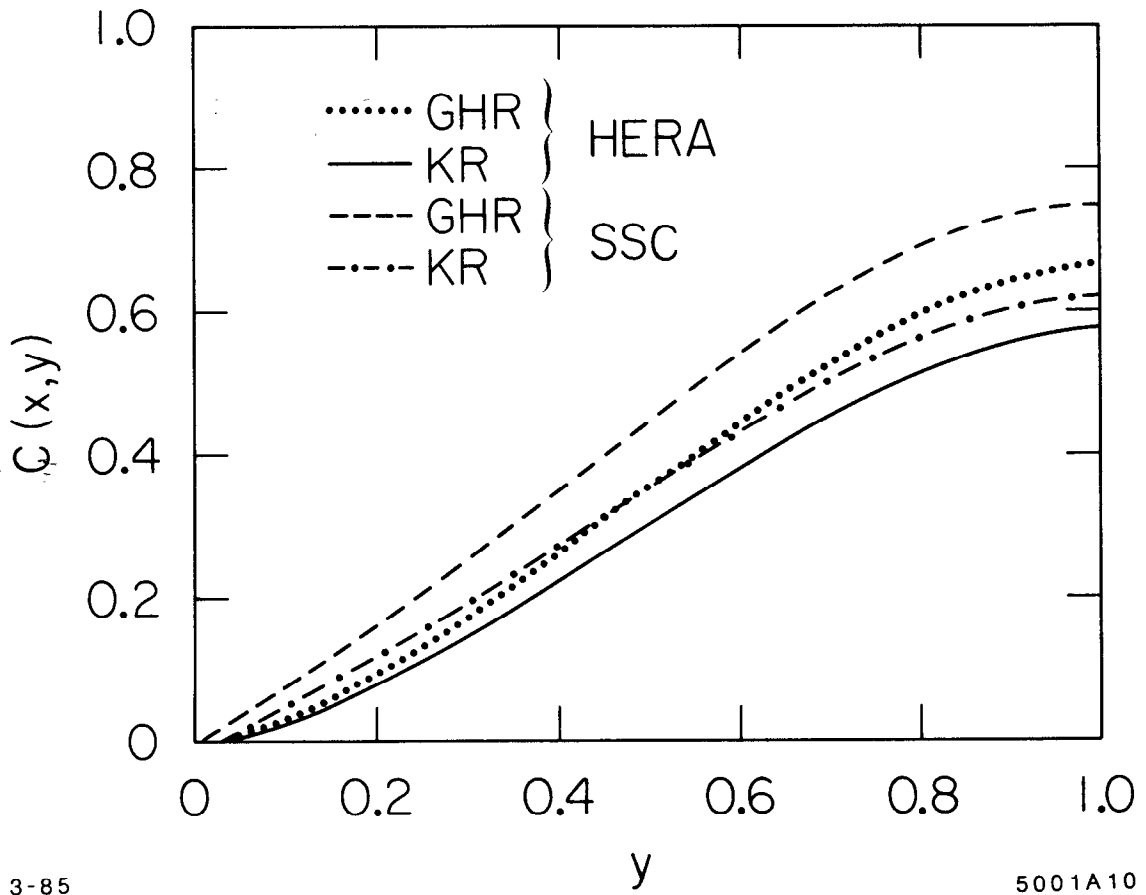
Fig. 4



3-85

5001A9

Fig. 5



3-85

5001A10

Fig. 6